Applied Catalysis B: Environmental 237 (2018) 835–843

Contents lists available at ScienceDirect

Applied Catalysis B: Environmental

journal homepage: www.elsevier.com/locate/apcatb

Improving stability of cyclopentanone aldol condensation MgO-based catalysts by surface hydrophobization with organosilanes

Duong T. Ngo, Tawan Sooknoi, Daniel E. Resasco*

School of Chemical, Biological and Materials Engineering, University of Oklahoma, Norman, Oklahoma 73019, USA

ARTICLE INFO

Keywords:
Aldol condensation
Cyclopentanone
Magnesium oxide
Nitrate-citrate combustion
Functionalization
Octadecyltrichlorosilane
Deactivation
Hydrophobization

ABSTRACT

Cyclopentanone is a promising building block in the conversion of biomass to fuels. It can be readily obtained from furanics derived from biomass and can be converted to intermediate products in the molecular weight range compatible with fuels via C–C bond forming reactions. Among them, aldol condensation is a promising route. Conventional MgO catalysts are intrinsically active to catalyze this reaction, but they usually exhibit low surface areas and low stability in the presence of liquid water. The nitrate-citrate combustion method results in high surface area oxides with high condensation activity, but they are still susceptible to water attack. Here, we show that hydrophobic MgO-based catalysts functionalized with octadecyltrichlorosilane (OTS) exhibit remarkable stability in the liquid phase under conditions in which a conventional MgO deactivates in short time.

1. Introduction

The combination of multistage thermal conversion of biomass and a catalytic cascade of C–C bond forming reactions followed by hydrodeoxygenation appears as an attractive strategy for the production of biomass-derived fuel components [1–5]. This strategy minimizes several drawbacks found in the more conventional pyrolysis/hydrotreating approach [6–10]. Furfural is among the most abundant components obtained from this multistage thermal conversion process [2]. While furfural is by itself an economically important aldehyde used in the synthesis of various chemicals [11–14], it is rather unstable and prone to coke formation, which causes rapid catalyst deactivation during upgrading. Recently, Hronec and co-workers [15,16] have called attention to an appealing path to produce a much more stable intermediate, cyclopentanone. That is, under hydrogen atmosphere and in the presence of water, furfural can be converted to cyclopentanone via the Piancatelli rearrangement combined with a two-step selective hydrogenation, before and after the arrangement; i.e., first, the −CO group in furfural is hydrogenated to −OH and then, the C=C double bond in cyclopentenone is saturated [17–21]. As a potential coupling agent, this non-toxic cyclic ketone has been utilized in the alkylation of phenolic compounds and, more particularly, the self-aldol condensation followed by hydrodeoxygenation to form bicyclopentyl, a promising fuel component [22]. A few attempts to optimize the catalysts that maximize C_5-C_5 coupling have been described in the literature, using both solid acids and solid bases [23,24]. Yang et al. [25] investigated the self-condensation of pure cyclopentanone at 150 °C on basic hydrotalcites and alkaline earth metal oxides and found high yields to 2-cyclopentylidenecyclopentanone. Likewise, Liang et al. [26] reported 100% selectivity to this dimer at 80% conversion over an MgO-ZrO_2 catalyst at 130 °C and 1 atm. Other authors have also used cyclopentanone as a co-reactant with aldehydes to obtain a broader range of fuel-range compounds. For example, the combination of cyclopentanone and furfural has been proposed by Ordonez et al. [27], using MgO-ZrO_2 as a catalyst operating under mild reaction conditions (20–50 °C) in an aqueous phase. At all furfural/cyclopentanone molar ratios (1:1 to 10:1), only cross-condensates were obtained due to the high affinity of furfural and the catalyst surface. Similarly, 2-cyclopentylidenecyclopentanone was also absent from the product mixtures in the study by Huber's group [28], who used solvent-free conditions for the reaction between cyclopentanone and butanal at 140 °C. Despite excess amounts of cyclopentanone and excellent activity of the solid base MgAl-HT, only cross-condensation products were obtained with 80% selectivity to cyclopentanone-activated adducts. Due to the very high yields and selectivity in which cyclopentanone can be produced from furfural [15,16], it is still interesting to investigate the production of the stable compound bicyclopentyl which may have desirable fuel properties [29–31].

The base-catalyzed self-condensation of cyclopentanone follows a nucleophilic addition (A_N) mechanism, in which the first step is the generation of an enolate intermediate resulting from the abstraction of a proton by the basic site from the C in the α position [32]. The second step that involves the C–C bond formation may occur either via reaction of an adsorbed molecule and a molecule in the fluid (Eley-Rideal

* Corresponding author.
E-mail address: resasco@ou.edu (D.E. Resasco).

https://doi.org/10.1016/j.apcatb.2018.06.044
Received 28 January 2018; Received in revised form 14 June 2018; Accepted 16 June 2018
Available online 18 June 2018

model) or via a bimolecular surface reaction (Langmuir-Hinshelwood model). In the first case, the enolate is bound to the surface while the electrophile is in the fluid phase [33,34]. By contrast, in the second case, the electrophile is also adsorbed [35]. The subsequent steps are C—C coupling, reprotonation, and dehydration. The resulting dimeric product (2-cyclopentylidenecyclopentanone) is also able to donate a proton to the surface for another condensation step that yields the trimeric product 2,5-dicyclopentylidenecyclopentanone.

MgO is a typical basic oxide commonly used in aldol-condensation and widely investigated [36]. While it is beneficial to enhance the surface area of MgO for higher reaction rates, this enhancement also enhances the uptake of undesirable nucleophiles such as water and product oligomers, which accelerate deactivation, as shown in several studies [25,37–39]. Finding catalytic materials that are effective for aldol condensation and at the same time more resistant to deactivation than conventional basic catalyst is an appealing objective. Therefore, the main goal of this contribution has been investigating novel materials with improved stability during aldol condensation. We have found that MgO, modified with mesoporous silica and subsequently grafted with an organosilane (e.g. octadecyltrichlorosilane) [40,41] that renders the surface hydrophobic, greatly improves catalyst stability.

2. Experimental methods

2.1. Synthesis of catalytic materials

2.1.1. Combustion method

2.1.1.1. MgO-NC. A mixture of 25.6 g of $Mg(NO_3)_2.6H_2O$ (Aldrich, 99.9%, 0.1 mol) and 30 mL of water was stirred vigorously for 15 min. at 80 °C. Then, a solution containing 19.2 g of citric acid (Aldrich, 99.5%, 0.1 mol) in 20 mL of water was added to the mixture, which was continuously heated and stirred until half of the liquid vaporized, leaving a viscous gel. This gel was subsequently calcined overnight under static air at 550 °C, during which time, combustion of the citric acid took place, producing a characteristic fluffy, high-surface-area MgO material [42,43], noted here as MgO-NC (for nitrate-citrate combustion).

2.1.2. Hydrophobization method

2.1.2.1. MgO@mSiO₂ composite. As demonstrated in previous investigations of analogous materials based on TiO_2 photo-oxidation catalysts [44,45], it is possible to enhance overall surface area without complete blockage of the active sites [46]. To prepare this hybrid material, 2 g of the parent MgO-NC were stirred vigorously for 15 min. at room temperature in a mixture of 4 mL of NH_4OH (50% v/v) and 40 mL of water. Subsequently, a 0.1 M solution of cetyltrimethylammonium bromide (CTAB) in a 1:2 vol. ratio of ethanol-water was added to the suspension, while continuously stirring for 30 min. Then, variable amounts of tetraethyl orthosilicate (TEOS) were introduced dropwise. The resulting suspension was stirred overnight, centrifuged, and washed 3 times with ethanol. The separated solid was dried at 100 °C overnight and calcined under static air at 400 °C for 6 h to obtain the $MgO@mSiO_2$ composite.

2.1.2.2. Functionalization with octadecyltrichlorosilane (OTS). The following method was used to hydrophobize the MgO-based materials. First, 0.45 mL of water was dropped onto 1 g of MgO-NC or $MgO@mSiO_2$, and the resulting wet solid was suspended in a 1:50 v/v OTS-toluene solution. Then, the suspension was shaken for 5 min. and stirred overnight, followed by centrifugation and three washes with ethanol. The separated solid was finally dried overnight at 110 °C to yield MgO-OTS (or $MgO@mSiO_2$-OTS), in which OTS has reacted with surface OH groups to generate a hydrophobic surface.

In this paper, we prepared two types of $MgO@mSiO_2$-OTS and one type of MgO-OTS with nominal compositions of (49 wt.% MgO - 21 wt.% SiO_2 - 30 wt.% OTS), (74 wt.% MgO - 10 wt.% SiO_2 - 16 wt.% OTS) and (70 wt.% MgO - 30 wt.% OTS) respectively. The catalyst with the first nominal composition, which was mainly used to study the catalytic activity and stability, is mostly referred to as $MgO@mSiO_2$-OTS for sake of simplicity.

2.2. Characterization

The final content of OTS in the $MgO@mSiO_2$-OTS sample was determined by thermogravimetric analysis (TGA). As MgO and SiO_2 are thermally stable under air, only OTS was quantitatively oxidized to CO_2 and H_2O, which were quantified by MS/TGA. For this purpose, 47.48 mg of $MgO@mSiO_2$-OTS was analyzed by heating with a linear ramp under a flow of an Ar-air mixture, starting from 40 °C and increased by 2 °C.min^{-1}.

Specific surface areas for samples MgO-NC, $MgO@mSiO_2$, MgO-OTS, $MgO@mSiO_2$-OTS, and commercial MgO were obtained on a Micromeritics 2010 instrument. The values obtained for $MgO@mSiO_2$ and $MgO@mSiO_2$-OTS were combined with mass spectra obtained during the TGA of the latter to quantify the distribution of OTS functionalities on the catalyst. For sake of simplicity, we assume complete hydrolysis of the chloro-groups in OTS and monodentate anchoring. Accordingly, $x = n_{OTS} \times N_A / A_{MgO@mSiO_2}$

where x = molecules of OTS, or $C_{18}H_{37}Si(OH)_2$-, anchored per unit area of $MgO@mSiO_2$ in $MgO@mSiO_2$-OTS; n_{OTS} = moles of OTS; N_A = Avogadro's number; $A_{MgO@mSiO_2}$ = surface area of $MgO@mSiO_2$.

The morphology of MgO-NC was analyzed by TEM (Zeiss 10 A). An SEM image of the final $MgO@mSiO_2$-OTS product was recorded in backscattered electron mode, combined with EDS analysis to determine whether the OTS had been fully hydrolyzed. X-ray diffraction (XRD) was used to assess the crystallinity changes of MgO initially prepared by the nitrate-citrate combustion, but later further treated in the presence of mesoporous silica.

The basicity of $MgO@mSiO_2$-OTS was characterized via temperature-programmed desorption (TPD) of adsorbed CO_2 following the method described elsewhere [47]. Briefly, in each run, 100 mg of $MgO@mSiO_2$-OTS was heated to 200 °C in the TPD system with a ramp rate of 10 °C.min^{-1}, under a He flow rate of 30 mL.min^{-1} and then cooled down to room temperature. A CO_2 flow rate of 30 mL.min^{-1} was then passed through the sample for 30 min., followed by a 2-hour purge with He to remove any physisorbed CO_2. The TPD was performed under the same He flow rate by heating to 600 °C with a ramp rate of 10 °C.min^{-1}.

2.3. Catalytic measurements

2.3.1. Aldol condensation under N_2

In each run, the solid catalyst (MgO-NC or $MgO@mSiO_2$-OTS) suspended in cyclohexane was placed into a 100 mL Parr reaction vessel. Before reaction, the system was purged with N_2, pressurized to 300 psig and heated to 150–200 °C. The cyclopentanone reactant was placed in a 30 mL feeding cylinder pressurized to 450–500 psig of N_2 along with an internal standard (toluene) and then injected into the reaction system, as soon as the desired temperature was stabilized. Reaction runs were carried out under a stirring speed of 750 rpm for a given reaction time. All liquids were analyzed by GC–MS and GC-FID as previously described [48].

2.3.2. Aldol condensation under H_2

Following a recently proposed approach [49], some of the aldol condensation runs were conducted in the presence of a Cu/SiO_2 catalyst under H_2. This method has shown to be effective in minimizing deactivation in the aldol condensation of acetone in the vapor phase [50]. In our case, 250 mg of 10 wt.% Cu/SiO_2 were placed into the 100 mL Parr reactor vessel along with the MgO-NC catalyst and the cyclohexane solvent. The system was then heated to 270 °C for 3 h under 500 psig of H_2 and cooled down to the reaction temperature of 150 °C. The

cyclopentanone feed was pressurized up to the target H_2 pressure in a 30-mL feeding cylinder along with toluene. As above, when the desired reaction temperature was stabilized, the feed was injected into the reaction system.

2.3.3. Quantification of the extent of catalyst deactivation

Catalyst deactivation during aldol condensation reactions is a common problem, which has been observed in numerous studies [25]. A common practice to model catalyst deactivation is to use an exponential decay of activity with time (t) according to the expression $a = a_0\, e^{-kD\, t}$, where k_D is the deactivation parameter, larger for rapidly deactivating cases and smaller for more stable catalysts. In a steady state, flow reactor, determining k_D is rather straightforward. However, evaluating deactivation in a batch reactor is much more complicated than on a flow reactor since the concentration continuously changes. And, both deactivation and reaction kinetics affect the variation of C with time. An effective method for comparing rates of deactivation in a batch reactor has been described by Apesteguia et al. [51,52]. In this method, the evolution of reactant concentration is plotted as a function of the product of catalyst mass and time (w x t) for two different amounts of catalyst. When there is no deactivation, the curves on the plot should coincide, but when the catalyst deactivates with time, the curves reach a plateau at different concentration values. That is, with a smaller amount of catalyst, a longer time is necessary to reach a certain conversion, thus the catalyst experiences more pronounced deactivation than in a run with the larger amount of catalyst, which for the same conversion has required a shorter period of time, with consequently lower extent of deactivation. The more different are the curves with varying catalyst amounts, the stronger is the extent of deactivation.

2.3.4. Reusability of MgO@mSiO$_2$-OTS

In addition to the deactivation test using C vs. (w x t) graphs, the stability of the catalysts was evaluated by re-using the catalysts in consecutive runs. In this experiment, 500 mg of the material was used for the first 2-hour reaction at 200 °C. After each cycle, the spent catalyst was washed with acetone, dried at 100 °C and saved for the next cycle, keeping the same reaction conditions. Evolution of conversion as a function of reaction cycle gave an estimate of the catalyst stability.

3. Results and discussion

3.1. Materials characterization

As depicted in Fig. 1, the TGA of MgO@mSiO$_2$-OTS exhibits two distinct mass losses. The first one, from 40 to 200 °C can be ascribed to the evolution of water, physically adsorbed on the surface; the second loss, with a maximum about 410 °C, is clearly due to the combustion of the functional groups in air. By quantifying the evolution of CO_2 and H_2O in this region, with the assumption that Cl is no longer present in the silanized surface and Si is not evolved during TGA, one can calculate the original loading of OTS in the as-prepared catalyst. The resulting value was about 20 wt.%, which is lower than the nominal 30 wt.% initially incorporated in the preparation, indicating that a fraction of the OTS initially added to the material is not effectively anchored and is lost during the post-synthesis washing steps in ethanol and centrifugation. However, the rest is strongly anchored and it can resist relatively high temperatures before it decomposes.

Table 1
Surface area, pore size, and pore volume of various MgO catalysts.

Catalyst	S_{BET} $m^2 \cdot g^{-1}$	Pore diameter nm	Pore volume $cm^3 \cdot g^{-1}$
MgO (commercial)	1.5	–	–
MgO-NC	97	9.5	0.22
MgO@mSiO$_2$	448	7.0	0.80
MgO-OTS	51	3.8	0.04
MgO@mSiO$_2$-OTS	173	4.8	0.19

Table 1 summarizes the specific surface areas of the various materials investigated. The MgO-NC sample prepared by the combustion method exhibits a surface area of almost 100 $m^2.g^{-1}$, more than fifty times greater than that of most commercial MgO samples, demonstrating the effectiveness of the nitrate-citrate combustion method to generate oxide particles of small size.

This value is further enhanced when the MgO particles are incorporated onto the structure of mesoporous silica. As shown below, when heated in the presence of mesoporous silica, the MgO particles redisperse and partially lose their crystallinity. Even more important for this work, a relatively high surface area is still retained on the hybrid material after functionalization with OTS. By substituting the TGA-based OTS content of MgO@mSiO$_2$-OTS and the BET surface area of MgO@mSiO$_2$ into the equation in Section 2.2, we have found that there is approximately one molecule of OTS attached to a nm^2 of MgO@mSiO$_2$, or as defined above $x = 1\ nm^{-2}$.

Fig. 2 shows the pore size distribution of the four samples. The original MgO material is composed of aggregates of non-porous MgO crystallites (see Supplemental Information A). Thus, the observed porosity is simply due to interparticle void spaces in the aggregates. Clearly, the incorporation of MgO onto the mesoporous silica enhances the overall porosity of the material and this porosity is partially retained upon functionalization with OTS.

To further characterize the structure of the different materials investigated, XRD was conducted on the three samples: MgO-NC, MgO@mSiO$_2$ and MgO@mSiO$_2$-OTS.

As shown in Fig. 3, the MgO-NC sample shows the typical XRD pattern of crystalline MgO (37.2°, 43.0° and 62.3°), thus verifying the identity and purity of MgO prepared via the nitrate-citrate combustion. By contrast, the subsequent method of incorporating the mesoporous

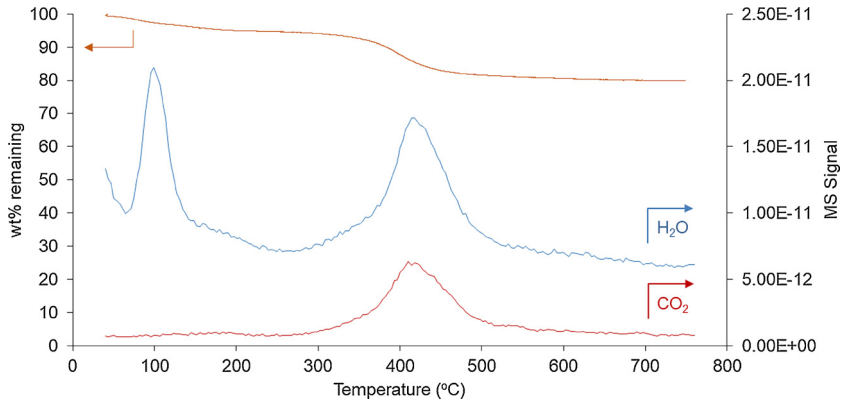

Fig. 1. TGA analysis and associated mass spectra of water and CO_2 evolved from the MgO@mSiO$_2$-OTS sample as a function of temperature.

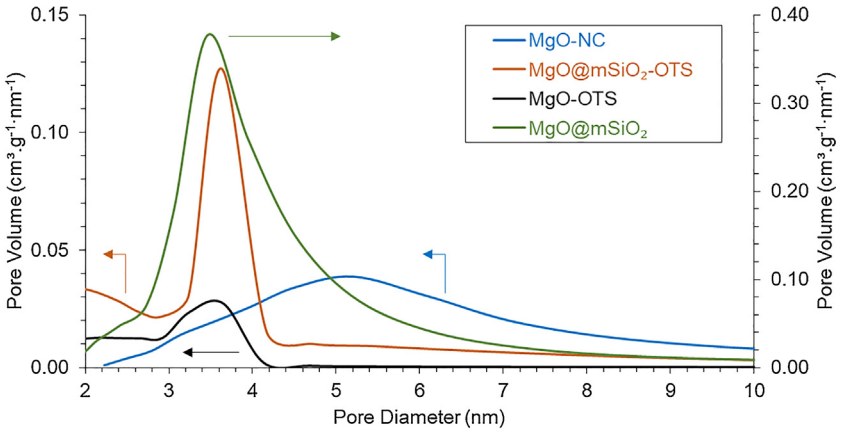

Fig. 2. Pore size distribution of functionalized MgO catalysts compared to the parent MgO prepared by combustion (MgO-NC).

silica into the system causes a drastic loss in crystallinity of MgO. As seen in the XRD pattern for the MgO@mSiO$_2$, the peak intensity is largely reduced and the peak width is broadened. That is, the vigorous stirring in aqueous NH_4OH, followed by interaction with TEOS and surfactant and final calcination at 400 °C, used to generate the hybrid MgO@mSiO$_2$ material cause significant alterations in the morphology and crystallinity of the MgO particles, resulting in redispersion and spreading of the MgO particles onto the silica surface. It is possible that during this procedure MgO may partially dissolve, re-precipitate, and perhaps interact with SiO_2 forming highly dispersed MgO domains. In fact, the elemental mapping obtained by EDS/SEM analysis (see Supplemental Information A) shows a very uniform distribution of Mg and Si. During the functionalization with OTS, the low crystallinity of MgO@mSiO$_2$ experiences a further decline, as indicated by the even lower intensity and further broadening of the MgO peaks.

To quantify the density of basic sites on the samples, we used the conventional TPD of adsorbed CO_2. As shown in Fig. 4, the MgO-NC sample exhibits two major desorption peaks, a smaller one centered at around 375 °C and a dominant peak centered at around 450 °C. In agreement with our previous report [47], this sample has a basic site density of 420 μmol.g^{-1}. The MgO@mSiO$_2$ sample exhibits a very similar TPD profile to that of MgO-NC, with a total basic site density of 390 μmol.g^{-1}, indicating that despite the dramatic changes in the topology of MgO, its surface chemistry remains unchanged after incorporation onto the silica surface. However, all of the sites of high basicity strength are eliminated following the OTS treatment, leaving a reduced basic site density of 240 μmol.g^{-1}, most of them in the region of intermediate basicity strength (i.e., the peak centered at 450 °C) with only a small peak remaining at around 500 °C, which reflects the presence of a small amount of strong basic sites.

3.2. Catalytic measurements

3.2.1. Apparent reaction order

In a batch reactor, it is important to decouple the kinetics from the catalyst deactivation. Therefore, to obtain the true reaction order, initial rates of cyclopentanone condensation were determined in 20-min runs over the MgO-NC catalyst at a constant temperature (150 °C) and varying initial concentrations of cyclopentanone. As shown in Fig. 5, the ln(initial rate) vs. ln(initial concentration) plot gives a straight line of a slope near 1.0, clearly showing the first order dependence of this reaction. This apparent order, displayed through a broad range of initial concentrations (0.2 M to 3.0 M), might suggest a unimolecular elementary step as the rate-determining step.

As mentioned above, the solid base-catalyzed A_N mechanism consists of aldehyde/ketone adsorption, α-proton abstraction (enolate formation), C—C coupling, surface proton abstraction (reprotonation), dehydration and product desorption. All of these steps but C—C coupling and reprotonation follow first-order kinetics. In several cases, such as the gas- phase self-condensation of propanal or acetone on anatase, enolate formation has been found to be rate-limiting [49]. Other rate-determining steps have been proposed in the literature to explain both, first- [53] and second-order kinetics [54,55].

3.2.2. Catalyst deactivation

To determine the extent of catalyst deactivation in the batch

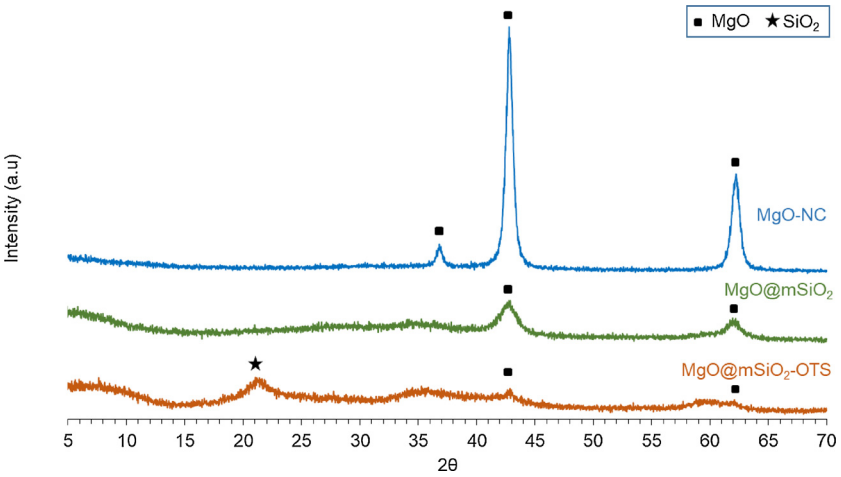

Fig. 3. XRD patterns of functionalized MgO catalysts compared to the parent MgO prepared by combustion (MgO-NC).

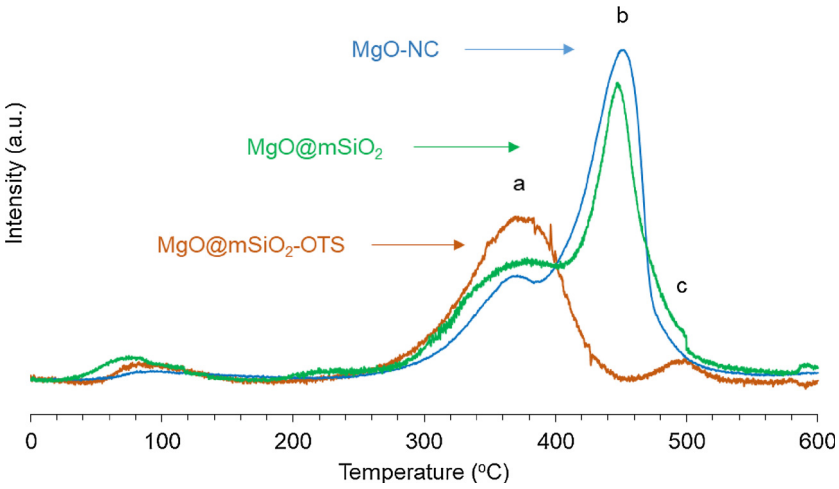

Fig. 4. CO_2-TPD on MgO-NC, MgO@mSiO$_2$ and MgO@mSiO$_2$-OTS.

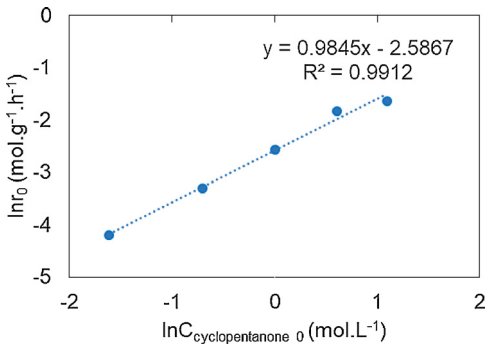

Fig. 5. Apparent reaction order for the self-condensation of cyclopentanone from initial rate measurements. Reaction conditions: 0.25 g of MgO-NC, 50 mL of feed, 150 °C, 450 psig of N_2, 20 min.

reactor, we followed the method described above [51,52] and plotted the variation of reactant concentration as a function of the catalyst mass x time product (w x t) using two different catalyst masses, namely w and 2 w. As shown in Fig. 6a, the curves for the as-prepared MgO-NC catalyst at 150 °C grow clearly apart as a function of w x t, indicating a rather large extent of catalyst deactivation. Clearly, the concentration of cyclopentanone no longer changes after a relatively short reaction time, indicating a zero rate.

To reduce the extent of deactivation, we conducted the reaction in the presence of 400 psia of H_2 with the addition of a Cu/SiO_2 co-catalyst to the liquid mixture. As seen in Fig. 6b, the gap between the two curves clearly narrows, indicating a lower extent of deactivation. As previously proposed [49], the presence of Cu/SiO_2 as a hydrogenation catalyst may saturate the C=C double bond of the product and a portion of the carbonyls to non-polymerizable ketones and alcohols, thus reducing coke formation. This explanation is supported by the observed product distribution (see Supplemental Information B) after 8 h, in which 2-cyclopentylcyclopentanone and 2-cyclopentylcyclopentanol are dominant C_{10} products. A shortcoming of this approach is the conversion of the cyclopentanone reactant to cyclopentanol in the presence of H_2, which leads to lower yields of the desired condensation product. By contrast, using a much lower H_2 pressure as that used in the gas phase experiments [50] results in a higher rate of catalyst deactivation. In fact, as shown in Fig. 6b, a large gap is observed between the conversions reached with 0.25 and 0.50 g of the catalyst after 480 and 240 min., respectively, for the runs conducted under 20 psia of H_2 on MgO-NC. As shown in the Supplemental Information C, while operating at this low pressure reduces the formation of cyclopentanol, allowing a higher concentration of the feed, the formation of the unsaturated dimer (2-cyclopentylidenecyclopentanone) is still observed, which may result in catalyst deactivation by coking. Therefore, for the cyclopentanone aldol condensation reaction, the simultaneous incorporation of H_2 and a hydrogenation catalyst may be detrimental to the rate of condensation. On the other hand, the hydrophobically modified catalysts MgO-OTS and MgO@mSiO$_2$-OTS show remarkable stability, even in the absence of H_2.

As can be seen in Fig. 6c and d, the curves of different catalyst masses for these samples lie very close, verifying the small extent of catalyst deactivation at both 150 and 200 °C. This is remarkable since the non-functionalized catalyst deactivates even faster at the higher temperatures. Interestingly, as illustrated in Fig. 6e, an increase in catalyst stability is also observed when the hydrophobization was directly conducted over the bare MgO substrate. In fact, as shown in Fig. 7a, within the first 8 h the catalytic performance of MgO-OTS is almost the same as that of MgO@mSiO$_2$-OTS. Beyond this time, MgO@mSiO$_2$-OTS shows a higher stability.

Fig. 7b makes a direct comparison of the change in reaction rate for the three catalysts. The unmodified MgO-NC exhibits much greater initial rates than the functionalized catalysts. However, the rate becomes essentially zero after less than 2 h. By contrast, while the initial rates over the hydrophobized MgO@mSiO$_2$-OTS and MgO-OTS catalysts are lower, the activity remains high for 32 h, reaching significant levels of conversion, eventually higher than that obtained on the non-functionalized catalyst.

Another important advantage of the functionalized MgO@mSiO$_2$-OTS catalyst is its tolerance to added water. Fig. 8 compares the effect of adding 2 mL of water to the 100 mL reaction mixture over the MgO-NC and MgO@mSiO$_2$-OTS catalysts. To make the comparison at similar conversions (16–18%) in the absence of water, the catalyst mass and reaction time were 0.25 g - 1 h for the former and 0.50 g - 4 h for the latter. As summarized in Table 2, the 2 mL of water added is significantly greater than the amount generated by the self-condensation reaction. The difference in the response to water addition is remarkable. While the MgO-NC sample lost 80% of its activity, the OTS-functionalized sample kept most of its activity in the presence of excess added water. In addition, these two catalysts were recovered after the reaction including external water and analyzed for morphological variation. Although Fig. 9 displays peaks attributed to crystalline Mg(OH)$_2$ from both samples, the XRD pattern of spent MgO@mSiO$_2$-OTS only slightly differs from that of the fresh one. On the other hand, there is a clear phase transition from MgO to Mg(OH)$_2$ with intensively distinct diffraction peaks on the spent MgO-NC. In other words, the 80% loss of activity of MgO-NC could be ascribed to the irreversible formation of Mg(OH)$_2$ following the exposure of MgO to 2 mL of added water.

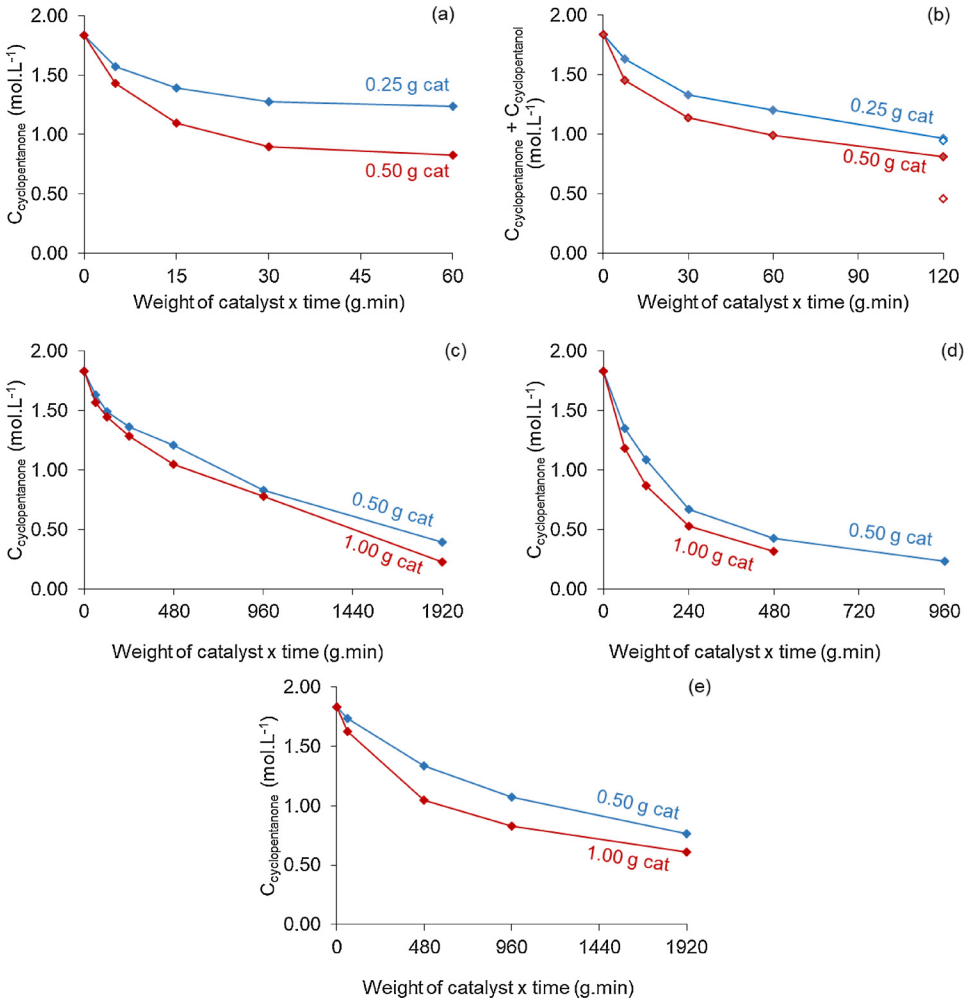

Fig. 6. Evolution of concentration with reaction time as a function of the (weight x time) product over various MgO catalysts (with masses of w and 2 w) to assess catalyst deactivation. (a) MgO-NC at 150 °C. (b) MgO-NC + 0.25 g of 10 wt.% Cu/SiO_2 (H_2) at 150 °C. Solid symbols – 400 psia of H_2. Open symbols – 20 psia of H_2. (c) MgO@mSiO_2-OTS at 150 °C. (d) MgO@mSiO_2-OTS at 200 °C. (e) MgO-OTS at 150 °C.

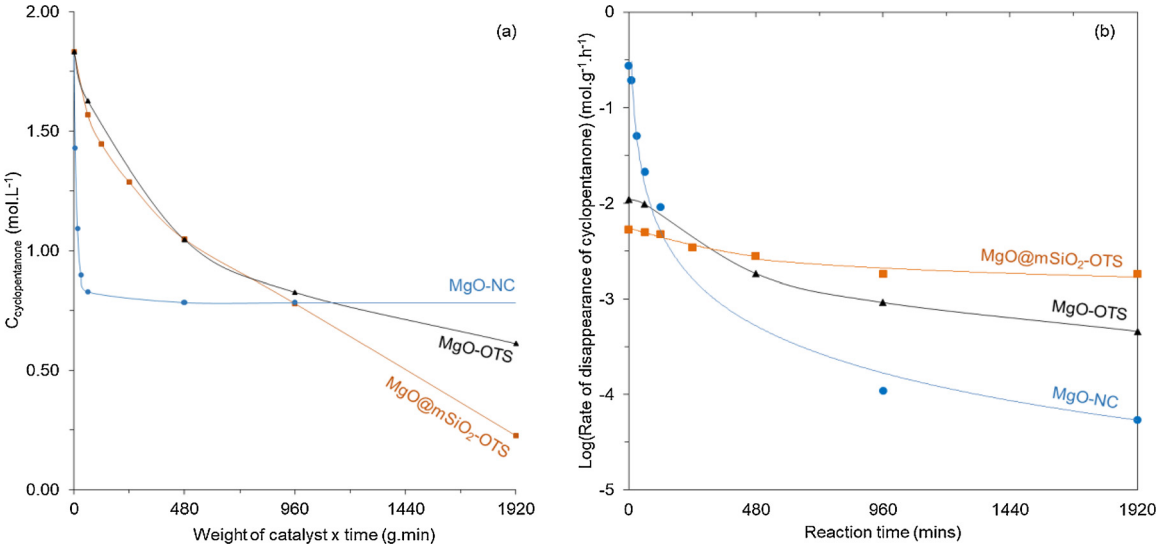

Fig. 7. Comparison of (a) reactant concentration profiles, and (b) reaction rates for the samples MgO-NC, MgO-OTS and MgO@mSiO_2-OTS catalysts at 150 °C in the batch reactor.

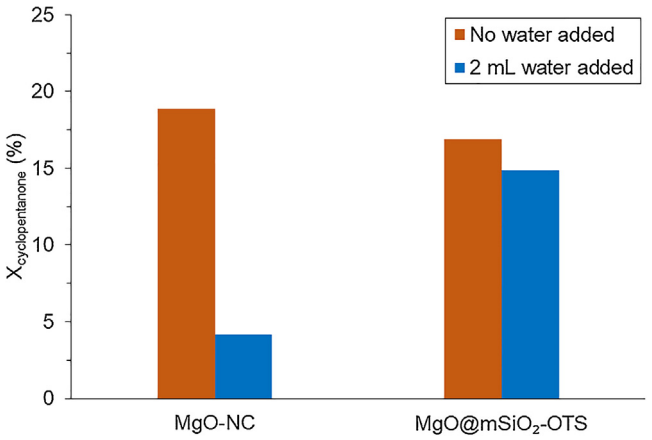

Fig. 8. Effect of external water on the catalytic activity of MgO-NC and MgO@$mSiO_2$-OTS. Reaction conditions: $C_{cyclopentanone\ 0}$ = 1.8 M, 150 °C, 450 psig of N_2, 0.25 g – 1 h for MgO-NC, 0.50 g – 4 h for MgO@$mSiO_2$-OTS.

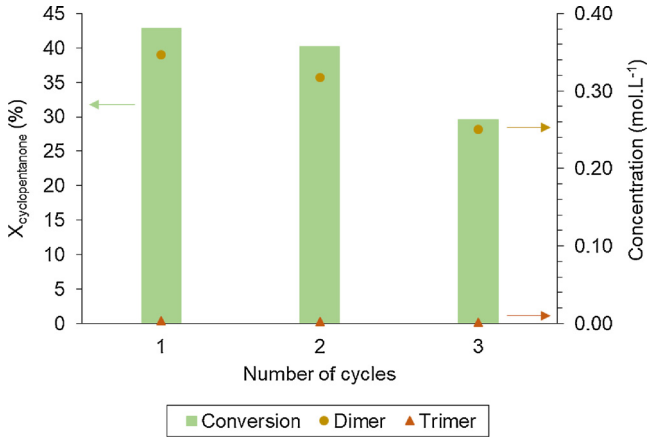

Fig. 10. Conversion and product distribution from consecutive uses of MgO@$mSiO_2$-OTS. Reaction conditions: 0.50 g of MgO@$mSiO_2$-OTS, $C_{cyclopentanone\ 0}$ = 1.8 M, 200 °C, 600 psig of N_2, 2 h.

Table 2
Different amounts of water involved in the self-condensation of cyclopentanone. Reaction conditions: $C_{cyclopentanone\ 0}$ = 1.8 M, 150 °C, 450 psig of N_2.

Catalyst	Weight g	Time h	$V_{H2O\ added}$ mL	$\Sigma C_{products}$ M	$V_{H2O\ formed}$ mL	ΣV_{H2O} mL
MgO-NC	0.25	1	0	0.16	0.15	0.15
	0.25	1	2	0.04	0.03	2.03
MgO@$mSiO_2$-OTS	0.50	4	0	0.15	0.14	0.14
	0.50	4	2	0.13	0.11	2.11

The positive effect of hydrophobization is also observed on the reusability of the catalyst after a reaction cycle. Fig. 10 shows the evolution of activity and selectivity of the MgO@$mSiO_2$-OTS during consecutive reaction cycles. Contrary to the relatively high reusability of the functionalized catalyst, the non-functionalized one (MgO-NC) loses all its activity after the initial cycle.

To rationalize the dramatic effect of the functionalization on catalyst stability, we have to analyze the differences observed in the surface characterization studies. The two obvious changes upon functionalization are the removal of the more basic sites in MgO and the conversion of a very hydrophilic surface into a hydrophobic one.

First, we can expect that the most active sites towards reaction with the Cl groups in the organosilane are the most basic sites. Therefore, eliminating the most basic sites should lower the initial activity, but prevent deactivation. In fact, it is seen that the sample with higher basicity (MgO-NC) exhibits higher initial activity but deactivates quickly. Also, as shown in Fig. 11, a significant amount of trimer (2,5-dicyclopentylidenecyclopentanone) begins to appear at higher conversions. It is conceivable that trimers and other larger oligomers can lead to accumulation of heavy carbonaceous compounds and catalyst deactivation. One of the additional effects of OTS functionalization is the inhibition of the formation of trimers. In fact, as shown in Fig. 11, the increase in the C_{trimer}/C_{dimer} ratio as a function of overall conversion is much greater on the non-functionalized MgO-NC than on any of the OTS-functionalized catalysts. The presence of silica does not seem to have a very significant difference, indicating that the silane functionalization is responsible for this change in selectivity.

Second, functionalization with a hydrophobic moiety has the obvious advantage of reducing the nucleation of water on the surface and formation of a liquid film that could block sites, cause mass transfer limitations, and even attack the MgO surface forming inactive $Mg(OH)_2$

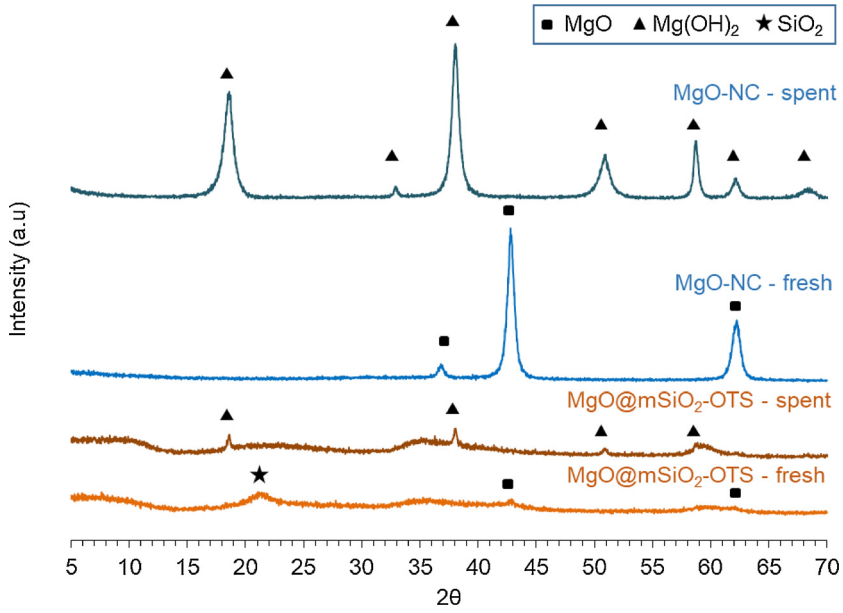

Fig. 9. XRD patterns of spent MgO and spent MgO@$mSiO_2$-OTS after exposure to 2 mL of water at 150 °C.

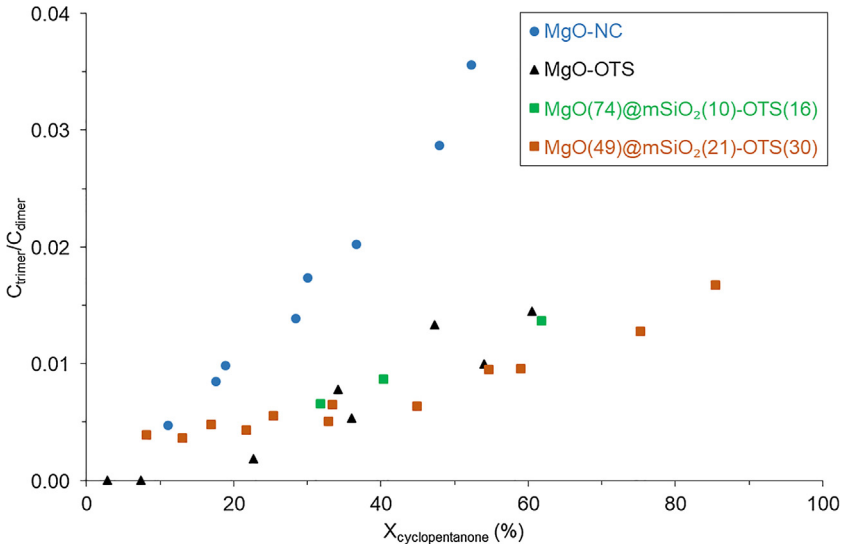

Fig. 11. The ratio of molar concentrations of the trimer and the dimer obtained from the MgO-catalyzed self-condensation of cyclopentanone with respect to its conversion. Reaction conditions: $C_{cyclopentanone\ 0}$ = 1.8 M, 150 °C, 450 psig of N_2.

[56,57]. One must notice that the aldol condensation reaction generates a water molecule for every α,β-unsaturated ketone. Since the solvent is non-polar cyclohexane, upon formation, water would tend to remain on the hydrophilic MgO surface, which would act as nucleation sites for the formation of a liquid film. Conversely, the hydrophobic surface of MgO@mSiO$_2$-OTS would not nucleate the formation of a liquid film, allowing water to phase-separate from the non-polar solvent, in line with the minimal effect on activity observed when large amounts of water were added to this catalyst, as shown in Fig. 8.

4. Conclusions

The main conclusions of the study are the following:

1 While MgO is an active catalyst for aldol condensation of cyclopentanone, it exhibits a low catalyst stability in the liquid phase, particularly in the presence of liquid water.
2 Functionalization with organosilanes increases the hydrophobicity of the surface, which has important effects on activity, selectivity, and stability. Specifically:
   a The catalytic activity is maintained for a much longer time than that of the non-functionalized material.
   b The resistance to water attack is greatly enhanced.
   c The initial rate is significantly reduced, most probably due to the selective titration of the most basic sites on the parent oxide.
3 Hydrophobization is more effective than other methods previously investigated for preventing deactivation of basic catalysts during aldol condensation. For example, while the addition of a hydrogenation catalyst is an effective method for other systems in the gas phase, such a method is less effective for cyclopentanone on MgO in the liquid phase. That is, at elevated H_2 pressures, ketone feed saturation reduces the overall rate of condensation. At low H_2 pressures, catalyst deactivation is significant.

Acknowledgements

This material is based upon work supported by the U.S. Department of Energy, Office of Science, Basic Energy Sciences under Award Number DE-SC0018284.

Appendix A. Supplementary data

Supplementary data associated with this article can be found, in the online version, at https://doi.org/10.1016/j.apcatb.2018.06.044.

References

[1] T.N. Pham, D.C. Shi, D.E. Resasco, Appl. Catal., B 145 (2014) 10–23.
[2] J.A. Herron, T. Vann, N. Duong, D.E. Resasco, S. Crossley, L.L. Lobban, C.T. Maravelias, Energy Technol. 5 (1) (2017) 130–150.
[3] D.E. Resasco, S.P. Crossley, Catal. Today 257 (2015) 185–199.
[4] N.N. Duong, B. Wang, T. Sooknoi, S.P. Crossley, D.E. Resasco, ChemSusChem 10 (13) (2017) 2823–2832.
[5] N. Duong, Q. Tan, D.E. Resasco, Comptes Rendus Chimie 21 (3-4) (2018) 155–163.
[6] L. Ivanhoe, World Oil 216 (10) (1995) 77–88.
[7] A. Bartlett, Math. Geosci. 32 (1) (2000) 1–17.
[8] H. Gluskoter, Increase in fossil fuel utilization in the twenty-first century: environmental impact and lower carbon alternatives, Div. Fuel Chem. Am. Chem. Soc., Preprints 44 (1) (1999) 36.
[9] G. Herbert, A. Krishnan, Renew. Sustainable Energy Rev. 59 (2016) 292–308.
[10] S. Czernik, A.V. Bridgwater, Energy Fuels 18 (2004) 590–598.
[11] D. Mohan, C.U. Pittman Jr, P.H. Steele, Energy Fuels 20 (2006) 848–889.
[12] P. Zapata, J. Faria, M. Ruiz, D. Resasco, Top. Catal. 55 (2012) 38–52.
[13] G. Huber, S. Iborra, A. Corma, Chem. Rev. 106 (2006) 4044–4098.
[14] D. Alonso, J. Bond, J. Dumesic, Green Chem. 12 (2010) 1493–1513.
[15] M. Hronec, K. Fulajtarova, Catal. Commun. 24 (2012) 100–104.
[16] M. Hronec, K. Fulajtarova, T. Liptaj, M. Stolcova, N. Pronayova, T. Sotak, Biomass Bioenergy 63 (2014) 291–299.
[17] C. Cai, T. Zhang, R. Kumar, C. Wyman, J. Chem. Technol. Biotechnol. 89 (1) (2014) 2–10.
[18] Y. Yang, Z. Du, Y. Huang, F. Lu, F. Wang, J. Gao, J. Xu, Green Chem. 15 (2013) 1932–1940.
[19] J. Guo, G. Xu, Z. Han, Y. Zhang, Y. Fu, Q. Guo, ACS Sustainable Chem. Eng. 2 (10) (2014) 2259–2266.
[20] M. Demirbas, Energy Sour., Part. A 28 (2006) 1181–1188.
[21] T. Pham, T. Sooknoi, S. Crossley, D. Resasco, ACS Catal. 3 (11) (2013) 2456–2473.
[22] M. Gollis, L. Belenyessy, B. Gudzinowicz, S. Koch, J. Smith, R. Wineman, J. Chem. Eng. Data 7 (1962) 311–316.
[23] G. Macala, T. Matson, C. Johnson, R. Lewis, A. Iretskii, P. Ford, ChemSusChem 2 (2009) 215–217.
[24] W. Shen, G. Tompsett, K. Hammond, R. Xing, F. Dogan, C. Grey, W. Conner, S. Auerbach, G. Huber, Appl. Catal., A 392 (2011) 57–68.
[25] J. Yang, N. Li, G. Li, W. Wang, A. Wang, X. Wang, Y. Cong, T. Zhang, Chem. Commun. 50 (2014) 2572–2574.
[26] D. Liang, G. Li, Y. Liu, J. Wu, X. Zhang, Catal. Commun. 81 (2016) 33–36.
[27] J. Cueto, L. Faba, E. Diaz, S. Ordonez, ChemCatChem 9 (2017) 1765–1770.
[28] J. Yang, S. Li, N. Li, W. Wang, A. Wang, T. Zhang, Y. Cong, X. Wang, G. Huber, Ind. Eng. Chem. Res. 54 (2015) 11825–11837.
[29] R.Y. Levina, V.R. Skvarchenko, O.Y. Okhlobystin, Zh. Obshch. Khim. 25 (1955) 1466–1469.
[30] M.B. Turovapolyak, I.E. Sosnina, E.G. Treshchova, Zh. Obshch. Khim. 23 (1953) 1111–1116.
[31] M.H. Gollis, L.I. Belenyessy, B.J. Gudzinowicz, S.D. Koch, J.O. Smith, R.J. Wineman, J. Chem. Eng. Data 7 (1962) 311–316.
[32] H. Kurokawa, T. Kato, T. Kuwabara, W. Ueda, Y. Morikawa, Y. Moro-Oka, T. Ikawa, J. Catal. 126 (1990) 208–218.
[33] R. West, Zh. Liu, M. Peter, C. Gartner, J. Dumesic, J. Mol. Catal. A: Chem. 296

(2008) 18–27.
[34] G. Solomons, C. Fryhle, Organic Chemistry, 7th edition, Wiley, New York City, 1999 p. 1264.
[35] M. Hasni, G. Prado, J. Rouchaud, P. Grange, M. Devillers, S. Delsarte, J. Mol. Catal. A: Chem. 247 (2006) 116–123.
[36] J.I. Di Cosimo, V.K. Diez, C. Ferretti, C.R. Apesteguía, RSC Catal. 26 (2014) 1–28.
[37] V. Chesnokov, A. Bedilo, D. Heroux, I. Mishakov, K. Klabunde, J. Catal. 218 (2003) 438–446.
[38] C. Perego, P. Villa, Catal. Today 34 (1997) 281–305.
[39] A. Saberi, F. Golestani-Fard, H. Sarpoolaky, M. Willert-Porada, T. Gerdes, R. Simon, J. Alloys Compd. 462 (1-2) (2008) 142–146.
[40] P. Zapata, J. Faria, M. Ruiz, R. Jentoft, D. Resasco, J. Am. Chem. Soc. 134 (2012) 8570–8578.
[41] M. Hronec, K. Fulajtarova, T. Liptaj, Appl. Catal., A 437-438 (2012) 104–111.
[42] A. Merzhanov, I. Borovinskaya, V. Yukhvid, V. Ratnikov, Scientific Principles of Material Science, Nauka, Moscow, 1981 p. 193.
[43] A. Varma, A. Rogachev, A. Mukasyan, S. Hwang, Adv. Chem. Eng. 24 (1998) 79–226.
[44] H. Pan, X. Wang, S. Xiao, L. Yu, Zh. Zhang, Indian J. Eng. Mater. Sci. 20 (2013) 561–567.
[45] T. Jesionowski, Pigm. Resin Technol. 30 (2001) 287–295.
[46] Z. Bo, T.R. Eaton, J.R. Gallagher, C.P. Canlas, J.T. Miller, J.M. Notestein, Chem. Mater. 27 (4) (2015) 1269–1277.
[47] T.N. Pham, L. Zhang, D. Shi, M.R. Komarneni, M.P. Ruiz, D.E. Resasco, J. Faria, ChemCatChem 8 (2016) 3611–3620.
[48] S. Sitthisa, T. Sooknoi, Y. Ma, P. Balbuena, D. Resasco, J. Catal. 277 (2011) 1–13.
[49] S. Wang, K. Goulas, E. Iglesia, J. Catal. 340 (2016) 302–320.
[50] S. Herrmann, E. Iglesia, J. Catal. 346 (2017) 134–153.
[51] V.K. Diez, C.R. Apesteguía, J.I. Di Cosimo, J. Catal. 240 (2006) 235–244.
[52] J. Zelin, A.F. Trasarti, C.R. Apesteguía, Catal. Commun. 42 (2013) 84–88.
[53] Z. Young, S. Hanspal, R. Davis, ACS Catal. 6 (2016) 3193–3202.
[54] S. Shylesh, D. Kim, A. Gokhale, C. Canlas, J. Struppe, C. Ho, D. Jadhav, A. Yeh, A. Bell, Ind. Eng. Chem. Res. 55 (2016) 10635–10644.
[55] K. Goulas, G. Gunbas, P. Dietrich, S. Sreekumar, A. Grippo, J. Chen, A. Gokhale, F. Toste, ChemCatChem 9 (2017) 677–684.
[56] S. Crossley, J. Faria, M. Shen, D. Resasco, Science 327 (2010) 68–72.
[57] T. Dossin, F. Reyniers, G. Marin, Appl. Catal., B 61 (2006) 35–45.